NASA TECHNICAL TRANSLATION NASA TT F-15,911

"MARS-3": PHOTOMETRIC PROFILES OF THE PLANET IN A NEAR-INFRARED SPECTRAL REGION

V. I. Moroz, A. E. Nadzhip, and V. S. Zhegulev

(NASA-TT-F-15911) MARS-3: PHOTOMETRIC PROFILES OF THE PLANET IN A NEAR-INFRARED SPECTRAL REGION (Scientific Translation Service) 39 p HC $5.00 CSCL 03B G3/30

N74-33274

Unclas 48458

Translation of "'Mars-3': Photometricheskiye Profili Planety v Blizhney Infrakrasnoy Oblasti Spektra". Institute of Space Research, Academy of Sciences USSR, Moscow, Report Pr-173, 1974, 37 pp.

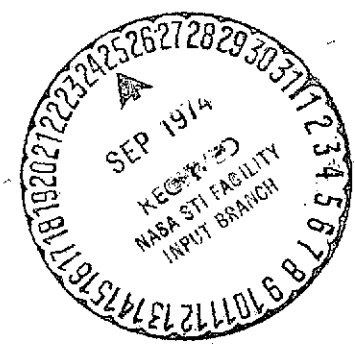

NATIONAL AERONAUTICS AND SPACE ADMINISTRATION
WASHINGTON, D. C. 20546 SEPTEMBER 1974

STANDARD TITLE PAGE

1. Report No. NASA TT F-15,911	2. Government Accession No.	3. Recipient's Catalog No.
4. Title and Subtitle "MARS-3": PHOTOMETRIC PROFILES OF THE PLANET IN A NEAR-INFRARED SPECTRAL REGION		5. Report Date September, 1974 6. Performing Organization Code
7. Author(s) V.I. Moroz, A.E. Nadzhip, and V.S. Zhegulev		8. Performing Organization Report No. 10. Work Unit No.
9. Performing Organization Name and Address SCITRAN Box 5456 Santa Barbara, CA 93108		11. Contract or Grant No. NASw-2483 13. Type of Report and Period Covered Translation
12. Sponsoring Agency Name and Address National Aeronautics and Space Administration Washington, D.C. 20546		14. Sponsoring Agency Code

15. Supplementary Notes

Translation of " 'Mars-3': Photometricheskiye Profili Planety v Blizhney Infrakrasnoy Oblasti Spektra". Institute of Space Research, Academy of Sciences USSR, Moscow, Report Pr-173, 1974, 37 pages.

16. Abstract

The brightness of Mars was measured in a narrow spectral interval at a wavelength of about 1.4 microns with a spatial resolution up to 5 km by means of a photometer on board "Mars-3". The measurement trajectories intersected the Martian continents, seas, and polar cap. The photometric profiles obtained along the trajectories contain a great many fine details related both to changes in the albedo and to surface inclinations. The photometric profiles of the continents are well described by the Lambert law. The sea-continent contrasts reached 0.5. It was found that they could be explained either by a difference in the particle dimensions (up to a factor of 3-4) or by the relative content of absorbing material (probably goethite). The optical thickness of dust clouds in the last period of a dust storm in 1971 was determined from the change in the sea-continent contrasts between December 1971 and February 1972. It was close to unity in regions close to the equator.

17. Key Words (Selected by Author(s))	18. Distribution Statement
	Unclassified - Unlimited

19. Security Classif. (of this report)	20. Security Classif. (of this page)	21. No. of Pages	22. Price
Unclassified	Unclassified	39	

ANNOTATION

The brightness of Mars was measured in a narrow spectral interval at a wavelength of about 1.4 microns with a spatial resolution up to 5 km by means of a photometer on board "Mars-3". The measurement trajectories intersected the martian continents, seas, and polar cap. The photometric profiles obtained along the trajectories contain a great many fine details, related both to changes in the albedo and to surface inclinations. The photometric profiles of the continents are well described by the Lambert law. The sea-continent contrasts reached 0.5. It was found that they could be explained either by a difference in the particle dimensions (up to a factor of 3-4) or by the relative content of absorbing material (probably goethite). The optical thickness of dust clouds in the last period of a dust storm in 1971 was determined from the change in the sea-continent contrasts between December, 1971 and February, 1972. It was close to unity in regions close to the equator.

"MARS-3": PHOTOMETRIC PROFILES OF THE PLANET IN A NEAR-INFRARED SPECTRAL REGION

V. I. Moroz*, A. E. Nadzhip** and V. S. Zhegulev*

1. Introduction

The brightness distribution on the disk of Mars depends on /3*** the photometric properties of the surface layer and, to a certain extent, on its composition and structure. Minnaert [1] proposed a simple empirical formula which is convenient for specifying the photometric properties of a planetary surface:

$$B = b_0 \mu_1^K \mu_2^{K-1}, \quad (1)^{****}$$

where B is the surface brightness,

μ_1 is the cosine of the angle of incidence;

μ_2 is the cosine of the angle of reflection;

K is a constant depending on the structure and composition of the surface;

$B_0 = \frac{E_0}{\pi} \rho_0$, where E_0 is the illuminance of a horizontal surface area perpendicular to the solar rays, and ρ_0 is the reflection coefficient for $\mu_1 = \mu_2 = 1$ (i.e., the normal albedo).

---

* USSR Academy of Sciences, Institute for Space Research.
** P. K. Shternberg National Astronomical Institute.

*** Numbers in the margin indicate pagination in original foreign text.

**** Translator's note. Symbol B_0 in (1) printed in error as b_0.

Formula (1) is one of the simplest functions of μ_1 and μ_2 which satisfy the Minnaert principle of reciprocity.

In the presence of an atmosphere, the total brightness of a planet is a composite of the atmosphere and surface brightnesses. Besides, the brightness of the surface is reduced by the atmosphere. In the case of small optical depth of the latter:

$$B = \frac{E_0}{\pi}\left\{\rho_0 \mu_1^{\kappa} \mu_2^{\kappa-1}\left[1 - \tau_0\left(\frac{1}{\mu_1} + \frac{1}{\mu_2}\right)\right] + \frac{\varkappa(\alpha)}{8}\tau_0\left(\frac{1}{\mu_1} + \frac{1}{\mu_2}\right)\right\}, \quad (2)$$

where τ_0 is the atmospheric optical depth;

α is the phase angle;

$\kappa(\alpha)$ is the scattering indicatrix.

For observations from Earth, with the planet in opposition, $\mu_1 = \mu_2 = \mu$, $\alpha = \pi$, and;

$$B = \frac{E_0}{\pi}\left[\rho_0 \mu^{q}\left(1 - \frac{2\tau_0}{\mu}\right) + \frac{\varkappa(\pi)\tau_0}{4\mu}\right], \quad (3)$$

where $q = 2k - 1$. The quantity q is called a smoothness factor. /4
N. N. Sytinskaya performed a large series of measurements of smoothness factors for natural terrestrial samples with the aim of identifying the Martian surface material according to its photometric properties [2].

For a surface obeying the Lambert law, $k = q = 1$. The parameter q, the normal albedo ρ_0, and the geometrical albedo ρ^* satisfy the simple relationship

$$\rho = \frac{2}{q+2}\rho_0. \quad (4)$$

Diffusely scattering surfaces with large reflection coefficients ($\rho_0 \approx 1$) are generally close to the Lambert coefficient in terms

---

*Translator's note: Inadvertently given in the foreign text as p.

of angular dependence. For dark surfaces with small values of ρ_0, the parameter q approaches zero. If ρ_0 is assumed constant on the planetary disk, then given absolute values of B at various point on the planet (with different μ), it is possible to obtain the quantity ρ_0, hence q, τ_0 and κ (α) by the method of least squares. This method was proposed by N. N. Sytinskaya [3] and V. G. Fessenkov [4], and has been subsequently repeatedly used in works by N. P. Barabashev, I. K. Koval, and their collaborators [5 - 7].

Briefly, the results are as follows. The normal albedo ρ_0 and parameter q in the visual region of the spectrum increase systematically toward long wavelenths. The normal albedo ρ_0 near 3500 Å is approximately 0.05. Near $\lambda \simeq 1$ micron, ρ_0 for the bright regions levels off at about 0.40, and does not increase at greater wavelengths. The parameter q accordingly also increases with increasing wavelength. Around 6500 Å it reaches 0.5 - 0.6. The difference in normal albedo between the dark and light regions is a maximum (about a factor of 2) in the red and near-infrared wavelength ranges, and practically vanishes in the blue. The optical depth of the atmosphere τ_0, on the contrary, decreases with increasing wavelength. In the red region of the /5
spectrum, the atmosphere (in normal state, in the absence of dust storms) does not significantly affect the brightness.

Earth-based photographic and photoelectric measurements of the brightness distribution on the Martian disk are unfortunately insufficiently accurate, due to poor spatial resolution. All published Earth-based photometry has a typical angular resolution limit of 1 arc second, corresponding to 300 km at the center of the disk even at the time of most favorable opposition.

Less definite results of photometric observations obtained with a spatial resolution of 5 - 10 km are available in the spectral region where the surface brightness has not been investigated at all — around 1.4 microns. These observations were performed using the photoelectric interferometric-polarimetric photometer IV-2 mounted on board the Soviet Martian space probe "Mars-3".

2. Instrument Details and Measurement Procedure

The chief purpose of the photometer IV-2 is determination of the water vapor content of the Martian atmosphere from the absorption line strength in the 1.38 micron band. The principle of operation of the instrument is described in another paper [8]. Here we only emphasize that use of the IV-2 instrument at these wavelengths also yielded brightness measurements in a wavelength interval of approximately 60 Å. The total equivalent width of the Martian H_2O lines amounts to less than 1 percent of the filter band width, and its effect on the measurement results can be neglected. One of the outputs of the photometer ("continuous spectrum channel") was an electrical signal proportional to the planet's brightness, transmitted by a telemetry system. The directional sensitivity pattern has a width of approximately 0.005 radian for a response of 0.5, which at a range of 1500 km corresponds to 7.5 km at the surface of the planet. The time constant of the instrument is 1.5 seconds. Measurement accuracy is 1.5 percent from the scale of the instrument. Practically the full scale was used. /6

The optical system of the IV-2 device includes a polarizing-interference filter and transmits only one polarized component of the continuous spectrum. However, the solar radiation reflected from the Martian surface in the near-infrared range is

polarized very weakly. On the basis of available Earth-based measurements [9], although these refer to slightly shorter wavelengths (to 1 micron) and to phases only slightly less than full (to 40°), one expects the polarization not to exceed a few per cent. Consequently, it is possible to exclude the effect of polarization from the analysis of results of the measurements.

The photometer IV-2 and other instruments in the astrophysics package were rigidly mounted in the body of the automatic interplanetary station (AMC) and oriented in a fixed direction during measurements, which was maintained by the vehicle's solar-stellar reference system. Near passage through the pericenter point of the orbit, the instrument was activated by optical sensors a few minutes before the limb was intercepted. The intercept occurred in the southern hemisphere (in the latitude zone 60 - 70°) and, thereafter, the optical axis scanned the surface along a line approximating a great circle (measurement scan path) for approximately 30 minutes, due to AMC motion. The scan paths were determined to an accuracy of 1 - 2° in areographic coordinates from the known vehicle trajectories. Additionally, in some cases these accuracies were verified by comparing the photometric profiles with "Mariner-9" photographs, and with a map based on the latter [10]. The location of the measurement paths is shown in Figures 1 - 4.

Measurements were made during seven pericenter passages. The first two, December 15 and 27, 1971, occurred at the time of /7
a dust storm, and the third (January 9, 1972) was not entirely free from its effects. The remaining four were made after the dust storm had ended (February 3, 16, 28, and March 12). Substantial portions of the February scans pass close to those of December, permitting a comparison of measurements during (specifically in the latter stages) and after the storm. The March 12

scan showed no definite relationship to the surface, and its position shown in Figure 1 is approximate.

At the beginning and end of a measurement sequence, a sensitivity calibration was performed. For this purpose, a standard lamp built into the photometer was activated for about one minute. It operated up to the first and after the second limb crossings. The calibration of the instrument during all measurement periods remained constant to within a few percent.

3. Observational Results

Figures 5 - 10 show the photometric profiles from seven measurement scans (December through January) plus data on the illumination and observing conditions (μ_1, μ_2, azimuth A). The phase angle during each observing period remained constant with values listed in Table 1. The scale of the cosine of the angle of incidence μ_1 was chosen to demonstrate how well the Lambert law ($k = q = 1$) approximates the brightness of the bright regions. The continents are not entirely uniform according to their brightness coefficient (note, for example, the February 16 profile shows the northern continents to be brighter than the southern ones). However, they are far more uniform than the seas. The Lambert law ($B \alpha \mu_1$) as can be seen in Figures 5 - 10, provides a sufficiently valid fit for the bright regions. A rigorous determination of the magnitude of K (from the slope of log $B \mu_2$ versus lg $\mu_1 \mu_2$) yields a value averaging slightly greater than unity (1.0 to 1.1), but it is uncertain that any significance can be attached to the difference. /8

TABLE 1. MEASUREMENT SCANS OF DECEMBER 15 - FEBRUARY: PHASE ANGLE, DISTANCE OF MARS FROM THE SUN, AND OTHER DATA*

Scans	Phase angle, α	Distance from Sun, Astronomical Units	Maximum value of μ_1	Brightness coefficient of the continents ρ_c	$\frac{\rho_c}{\rho_{c(28.02.72)}}$
December 15, 1971	52	I,44I	0,695	0,45	I,I0
December 27, 1971	53	I,456	0,7I5	0,43	I,05
January 9, 1972	54	I,473	0,727	0,42	I,02
February 3, 1972	56	I,505	0,826	0,44	I,08
February 16, 1972	57	I,52I	0,876	0,42/x	I,03/x
February 28, 1972	59	I,537	0,934	0,4I	I,00

*Commas represent decimal points.

/xApproximation of the smoothed photometric profile by the Lambert law is ambiguous for this date.

The scan of December 15 begins at the point ($\varphi = -56^0$, $\lambda = 356^0$). At first, the intersection of the optical axis with the surface proceeds along the tract very fast; then its speed decreases, and approaches the orbital velocity of the space probe. The first five minutes the path moves in the eastward direction through the latitude zone 60 - 67°, then turns toward the northeast. Initially the Sun is situated toward the East, then it gradually swings toward the South. Near longitude 290°, it is in the meridian (local noon), then sinks toward the West. Near the /9
Equator, the track crosses the terminator, and beyond here passes into the nighttime region of the planet. In the longitude zone 280 - 240°, the track crosses one of the little-studied dark areas of the southern hemisphere, Promethei Sinus. Its photometric profile is quite peculiar. A few minima of this profile (u, a,

in Figure 5) may be related to the slopes of crater walls (u, a, in Figure 2). Around latitude - 40° is the eastern border of Mare Tyrrhenum; then comes Mare Cimmerium, whose northern boundary is intercepted near latitude - 14°. It must be noted that the borders of the dark areas delineated on maps produced from Earth-based observations, agree with out photometric profiles to very high accuracy in general (within a few degrees). On our profiles, the seas, as a rule, are "wider" by 2 - 3°, which is explained by the high accuracy of measurements — the darkening becomes evident earlier; the borders of the seas are shifted toward the bright areas.

The photometric profiles of Mare Tyrrhenum and Mare Cimmerium are much smoother in the scans of February 15, than the profile of Promethei Sinus. The smooth character of the former was evidently connected with dust clouds which reduced the contrast. From a comparison with the profiles obtained at earlier dates (December 15, December 27, January 29, corresponding to Figures 5, 6, 7, respectively), it can be seen how the profiles of the seas all become deeper and more irregular.

The December 27 and January 9 tracks are each very similar, in their position on the map, to that of December 15, except that they are displaced by 90° and 180°, respectively. They initially traverse southern dark areas (Mare Australe, Depressio Hellespontica), move across a narrow "continental" region, then enter seas in the equatorial zone. /10

The scan of February 3 was only partially used for technical reasons. The scientific instruments were turned off within nine minutes after intercepting the limb. The initial portion of the tract crossed continental regions entirely; then a decline in brightness began in the area of Mare Cimmerium, and the readout is terminated.

The motion of Mars in its orbit and the evolution of the orbit of the probe progressively alter the nature of the scans. The initial points move northward, precisely northwestward. The terminator is no longer crossed, and the scan paths are entirely situated in the daytime region of the planet. But, on the other hand, areas lying in high northern latitudes are traversed, up to nearly 65 - 70° north latitude. On the scans of February 16 and 28, there are such small continental segments that their approximation as Lambertian is not very valid (particularly, February 16). Here, as well as on the previous scans, a certain amount of the details in the photometric profiles correspond to peculiarities in the relief (chiefly craters) discovered by "Mariner-9".

At latitudes above 40°, in the second half of February, the surface was cloud-covered, judging from the Mariner photographs and "Mars-3" photometric profiles obtained in the 0.36 - 0.5 micron wavelength range. These clouds, bright in the near-ultraviolet range, were entirely imperceptible on the above-mentioned profiles and, consequently, have a small optical depth at a wavelength of 1.4 microns.

The contrast between the seas and continents on December 15 and 27 is evidently reduced in level from that of February 3 and 16, if those areas with similar coordinates are compared. This comparison is presented in Table 2. Here the values of the brightness coefficient $\rho = (\pi_1 B)/(E_0 \mu_1)$ are listed for nearby areas of the planet for each pair of corresponding dates, plus longitudes, latitudes, and cosines of the photometric angles for these areas. The contrasts are given by the relation $K = (B_c - B_m)/B_m$, where B_m is the brightness of the sea (solid curve) B_c is the brightness of the continent (dashed curve, giving the /11

TABLE 2. COMPARISON OF CONTRAST DURING AND FOLLOWING THE DUST STORM*

Region	Date	φ	λ	μ_1	μ_2	ρ_m	ρ_c	κ
Mare Cimmerium	12/15/71	-30	222	0,457	0,976	0,35	0,45	0,22
	2/3/72	-30	215	0,826	0,855	0,28	0,44	0,36
Iapygia	12/27/71	-26	304	0,535	0,992	0,30	0,43	0,30
	2/16/72	-25	299	0,872	0,816	0,23	0,42	0,45

*Commas represent decimal points.

interpolated Lambertian brightness level corresponding to the continents). Evidently, the contrast in the period of the dust storm was reduced by 50 percent. This latter fact may be utilized to estimate the size of the dust particles [11, 12].

The atmospheric transparency during the dust storm evidently varied with latitude. At 50° south latitude, on the scans of December 15 and 27, the brightness profiles contain a large amount of fine detail, while at the same time there are no details nearer to the Equator. The seas appear as shallow minima.

According to the degree of settling of the dust simultaneous with an increase in contrast, the brightness coefficient of the continents only slightly decreased. Table 1 gives the brightness coefficient for the continents normalized to February 28. These results were computed taking account of the reduced distance from the Sun. The table shows that during the period of observation the value decreased by only 10 percent.

For February 28, we adopted a normal albedo $\rho = 0.41$, the typical value for the bright regions of the planet in a calm, /12
stormless period. It is taken from Earth-based observations in

the work of McCord and Westphal [13], with the qualification that there it is incorrectly given as the geometric albedo. Taking the absolute value $\rho_c = 0.41$ for February 28, we found ρ_c for all the remaining dates listed in Table 1. In similar fashion, the absolute brightness scale for our measurements was obtained (to the left along the ordinates of Figures 5 - 10).

Typical of all the profiles of the latter calm period (as well as for the southern portions of the December 15 and 27 profiles) are narrow brightness minima, sometimes having large contrast. The widths of these peaks are a few tens of kilometers. In many cases, they may be explained by slopes, i.e., local variations in μ_1. For example, the dark feature a on the scans of December 15 and February 3 appeared first of all upon crossing the identical crater located near $\varphi = 51°$, $\lambda = 242°$ (Figure 2). The half-width of this feature (in the profile) is 10 seconds, corresponding to $\approx$ 40 kilometers. An inclination to the horizontal of approximately 3°, based on an approximate estimate, is sufficient for the observed brightness decrease.

In certain places, sharp brightness minima occur that are difficult to attribute to slopes. For example, on the scan of February 16, the minimum at latitude - 47°, if related to a slope, leads to an angle of 20° over a base length of 30 - 40 km, which can hardly be real. These details have an "albedo" origin. On the February 16 profile, some ten dark details coincide closely in position with craters discovered by "Mariner-9" (Figure 3).

4. On the Nature of Dark Areas

The difference between the dark and light areas is almost unrelated to particular differences in relief. Thus, so-called "craterless" areas always appear bright, but the possibility is /13

not excluded that their "craterlessness" is explained by local dust storms. Since this is concerned mostly with the extent of the cratered form of relief, the dust storms are equally plausible reasons for its distribution between the dark and light regions.

For a long time, the question has been discussed whether the dark areas are higher or lower than the bright areas. Altimetry based on CO_2 bands performed by "Mars-3" shows the dark areas tend to be higher than the bright areas [14].

Sagan and his co-authors [15] note that dark spots ("splotches") on the Mariner photographs with sizes of a few tens of km occur more frequently in the seas. However, these occupy much too small a fraction of the total area to explain the total albedo difference between continents and seas. The average reflectivity of the sea-covered surface is unquestionably lower than the continental, and intermediate between the latter and the "splotches".

Periodic dust storms reveal the presence of finely granulated material on the Martian surface. Concerning this, the results of infrared radiometry have been independently discussed (cf., e.g., [16], [17]). Thus, it is natural to consider that the simplest optical model of the Martian soil is a limited horizontal surface of a semi-infinite medium consisting of fine particles which scatter and absorb. From a consideration of the atmospheric aerosols consisting of granules of the same size, such a medium will be distinguished by a much higher packing density. At a sufficient packing density, the effect of diffraction becomes negligible, but, on the other hand, the effect of geometrical screening of one particle by others arises [18]. The latter leads to the appearance of a spike in the reflectivity

at small phase angles. At phase angles around 50°, the screening effect is negligible, and one can derive the photometric properties of the surface from the usual relations for optically scattering media, provided that full account is taken of the fact that at high packing density, the effective values of the single-scattering albedo and scattering indicatrix are altered, due to the vanishing or weakening of diffraction effects. According to an approximate theory for scattering of radiation in optically thick layers, developed by G. V. Rosenberg [19], the brightness coefficient of a homogeneous medium averaged over azimuth is given by /14

$$\rho(\mu_1, \mu_2, a, x_1) = h e^{-4S\sqrt{\frac{1-a}{3-x_1}}}, \quad (5)$$

where a is the single scattering albedo;

$x_1 = \frac{3}{2}\int_0^{\pi} x(\gamma)\cos\gamma\sin\gamma\,d\gamma$ is a parameter characterizing the elongation of the scattering indicatrix ($x_1 = 0$ for a spherical indicatrix, $x_1 \to 3$ for a very elongated one);

h is the brightness coefficient for a = 1 (all other parameters of the medium are retained); h is a function of x_1, μ_1, μ_2, differing slightly from 1;

S is a function of x_1, μ_1, μ_2, also differing only slightly from unity.

V. V. Sobolev [20] gives the expression for the "reduced" albedo (the latter being the result of averaging ρ over μ_2):

$$\tilde{\rho} = 1 - 4\sqrt{\frac{1-a}{3-x_1}}\,u_0(\mu_1), \quad (6)$$

where $u_0(\mu_1)$ plays a role analogous to S. Both expressions are identical for small values of $\sqrt{\frac{1-a}{3-x_1}}$.

For spherical particles with not too large a refractive index ($n < 2$), and with sufficiently large radii,

$$r > \frac{\lambda}{\pi} \frac{1}{n-1} \quad (7)$$

the albedo for single scattering is expressible in the following way: /15

$$a \simeq (D+R) + (1-D-R)\, e^{-\frac{4}{3} K r} \quad (8)$$

where D is the fraction of the diffracted light, and R is the fraction reflected; K is the volume absorption coefficient of the material; r is the particle radius. For light packing $D \sim 0.5$, and, due to the small n, $R << D$. With dense packing, in cases where the diffraction effects vanish,

$$a = R + (1-R)\, e^{-\frac{4}{3} K r} \quad (9)$$

According to Irvine [18], the particles can be considered densely packed, and diffraction neglected when

$$r \gg \sqrt{\frac{\lambda}{\sigma n}}, \quad (10)$$

where σ is the extinction cross section; n is the concentration. For dense packing in a cubic lattice ($n = 1/8\ r^{-3}$) and cross section $\sigma = 2\ \pi\ r^2$, Formula (10) yields a still simpler criterion:

$$r \gg \lambda. \quad (11)$$

The parameter κ_1 depends only weakly on radius for sufficiently large particles. It varies within the limits 2 to 2.5, provided Condition (7) is met.

It appears most probable, upon consideration of simple models, that the difference in ρ between the dark and light

regions is explained as primarily due to a difference in a. The latter, in turn, may have two causes: 1) a difference in radii; 2) a difference in absorption coefficients.

Figure 11 shows the dependence of the single scattering albedo and reduced albedo $\overline{\rho}$ on the absorption coefficient and particle radius. Two sets of curves were derived from Equations (8) and (9). It was assumed that D = 0.5 and R = 0. The dependence of $\overline{\rho}$ on 1 - a was calculated from Equation (5) for the cases h ≡ 1, S ≡ 1, κ_1 = 2.0. Horizontal lines indicate the levels $\overline{\rho}$ = 0.40 and 0.20, corresponding to the continents and darkest seas. /16

The relation obtained imposes additional limitations on the possible composition and radii of the particles of the Martian soil. There are many indications that the reddish color of Mars and various other optical properties of its surface are attributable to the presence of goethite (limonite) $Fe_2O_3 \cdot nH_2O$ (cf., e.g., [21 - 23]). On the other hand, the Martian soil contains not less than 50 percent SiO_2 [24]. It is natural to consider a hypothetical composition of a mixture of limonite and various types of silicates. Figure 12 gives the dependence of the absorption coefficient at λ = 1.4 microns on the goethite content in mixtures of goethite + basalt and goethite + obsidian. The optical constants of the adopted minerals were taken from [25, 26]. A comparison of the curves in Figures 11 and 12 leads to the following conclusions:

1) In goethite + basalt mixtures, particles with radii greater than 2 microns for the bright regions and 8 microns for the dark regions are excluded.

2) In goethite + obsidian mixtures, particles with radii greater than 30 microns for the bright regions and 100 microns for the dark regions are excluded.

3) If an identical particle radius is adopted for the continents and seas, the relative goethite content in the soil of the seas is 3 - 4 times greater than in the continental soil.

4) If an identical soil composition is adopted for the continental and sea regions, the radius of the particles in the sea regions is 3 - 4 times greater than in the continental.

5) If particle radii approximately 1 micron are adopted (as for the dust clouds [11, 12, 27]), then the relative abundance of goethite in the continental regions amounts to roughly 10 percent.

Infrared radiometry in the $\lambda > 8$ micron band yields a mean particle radius of about 100 microns, with local variations of greater as well as smaller sizes [16, 17]. These local variations are uncorrelated with albedo, and consequently particles of such great sizes cannot account at all for the observed intensity of the scattered radiation, unless they have a fine structure on a micron scale. Thus, the available data indicate a composite structure of the surface layer: it probably consists of quite large particles (radii of tenths of a millimeter), composed in turn of micron-sized particles [28]. /17

5. Optical Depth of the Clouds During the Dust Storm

This quantity can be evaluated from measurement of the contrast between the dark and bright regions, data for which are given in Table 2. In the period of a dust storm, we can no longer consider the atmosphere as optically thin and, therefore, neglect its influence. Formulas of types (2) and (3) are useless here. It is necessary to apply the theory of light scattering in an optically thick atmosphere in the presence of an underlying layer. For approximate evaluations, the asymptotic formulas already frequently used above to evaluate the optical properties of the soil are convenient. According to [19], the brightness coefficient of a scattering atmosphere, having a finite optical thickness τ_0, and situated above an underlying surface whose albedo is A_n, equals

$$\rho = he^{-4sy} - g(\mu_1)g(\mu_2)\frac{shy}{sh\delta y}\left[e^{-\delta y} - \frac{An\,shy}{sh\delta y - An\,sh(\delta-1)y}\right], \qquad (12)$$

where $y = \sqrt{\frac{1-a}{3-x_1}}$, $\delta = \frac{\tau_0}{4}(3-x_1)+1$, $g(\mu)$ is the angular dependence of the transmission coefficient. The first term of this expression is equivalent to (5); but refers here to scattering in the atmosphere and not in the soil. As before, we set $h \equiv 1$, $S \equiv 1$. For values of $g(\mu)$, we utilize, from [20], the approximate relation

$$g(\mu) = \frac{1}{2} + \frac{3}{4}\mu_0, \qquad (13)$$

which gives for both cases listed in Table 2, $g(\mu) = 1.1$. /18

Figures 13 and 14 give values of ρ, computed as a function of $\tau_0(3-x_1)$, for values of $\frac{1-a}{3-x_1} = 0.040$ and 0.025. The former yields the maximum brightness coefficient 0.45 actually observed

on December 15. The latter case was studied in order to assess the influence of a variation of the parameter $\left|\frac{1-a}{3-x_1}\right|$ on the results.

From an inspection of Figure 13, it follows that the observed changes in Mare Cimmerium, between December 15 and February 3, require for the first case $\tau_0 \simeq 1.2$. In the second case, the value $\left|\frac{1-a}{3-x_1}\right|$, which is almost reduced by half, changes τ_0 by at most 20 percent. For December 27, as necessarily expected, an optical thickness slightly less than that of December 15 is obtained.

The results of this calculation procedure contain a certain amount of uncertainty in connection with the fact that similar, but at the same time entirely different, regions of the seas are compared. Therefore, it is of interest to repeat them, comparing the mean contrast of the darkest sea regions in the scans of December 15 and 27 (about 0.30) with January 9, 16, and February 28 (0.45 - 0.50). From this we also obtain $\left|\tau_0(3-x_1) \simeq 1\right|$.

As mentioned earlier (Section 2), the photometric profiles of the seas in the dust storm period appear not only "shallower", but substantially smoother. This difference in the degree of smoothness is very marked: the amplitude of small fluctuations in brightness from the mean for the February observation series is 3 - 5 times greater than for the December series (in the latitude zone north of - 40°). If the fluctuations have an "albedo" cause, then for such weakening, as seen from the curves in Figures 13 and 14, $\left|\tau_0(3-x_1)\right|$ must be not less than 3. But in this case, the average contrast of the seas is also reduced more strongly than the observations indicate. Evidently, the fine structure of the photometric profiles is basically related to

slopes, and we have the possibility of statistically analyzing the latter from the photometric data obtained after the end of the dust storm. /19

The authors consider it their pleasant duty to express their appreciation to colleagues who rendered essential assistance at various stages of completion of this work, among them F. A. Korolev, A. Yu. Klement'yev, T. S. Meshcheryakov, Ye. V. Mashintsev, K. A. Tso, V. G. Butkevitch, Yu. A. Malyugin, O. G. Taranov, A. A. Liberman, V. G. Bukhin, and A. N. Repin.

The authors also acknowledge D. Schneiderman (NASA) for making available to Soviet scientists Mariner photographs of regions situated adjacent to the "Mars-3" measurement scans, and all American colleagues who participated in their preparation.

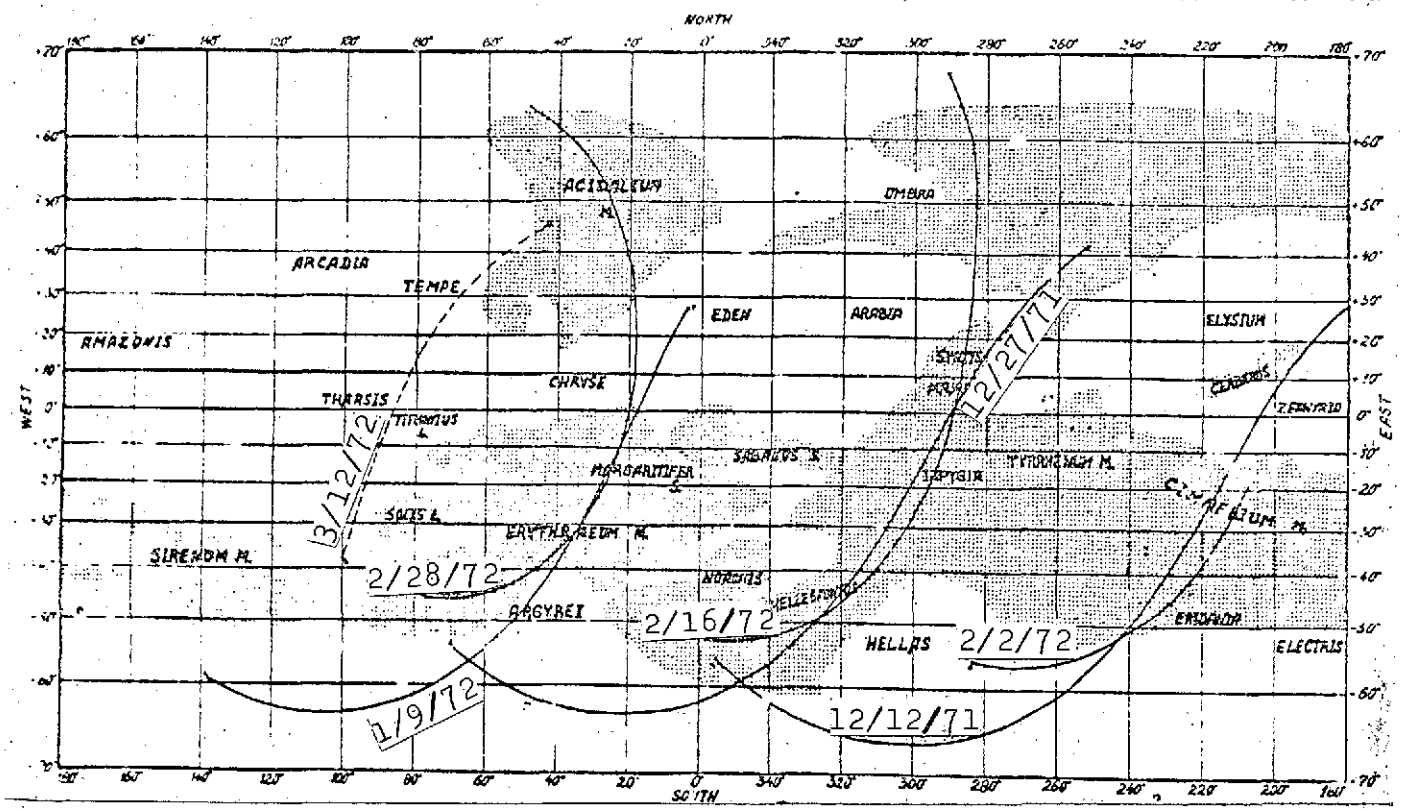

Figure 1. Schematic "albedo" map of Mars showing the measurement scan paths. Positions of the seas are labeled

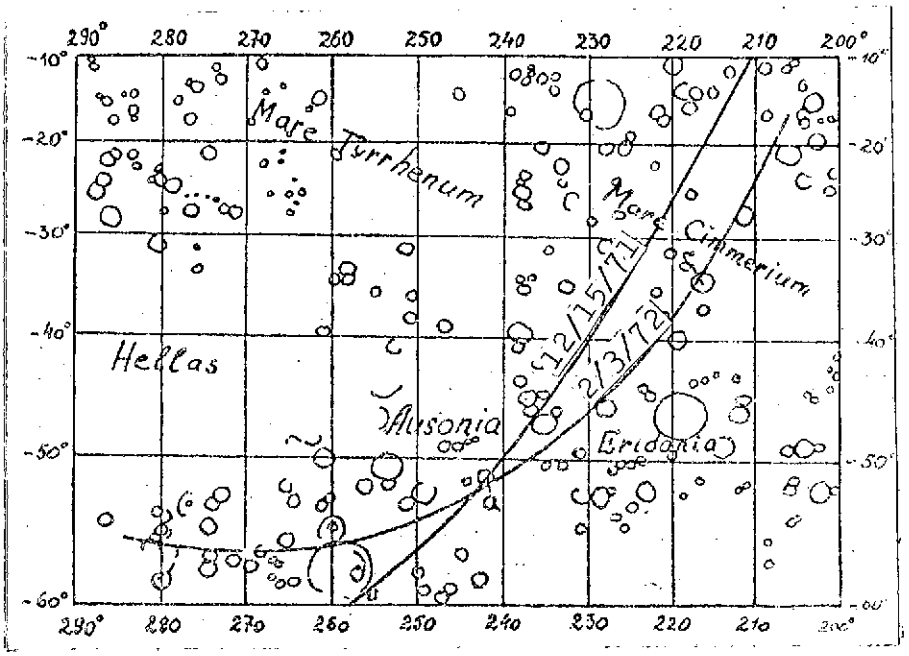

Figure 2. Distribution of topographic details on the Martian surface (from the "Mariner" map [10]) in the area of the scans of December 15, 1971 and February 3, 1972

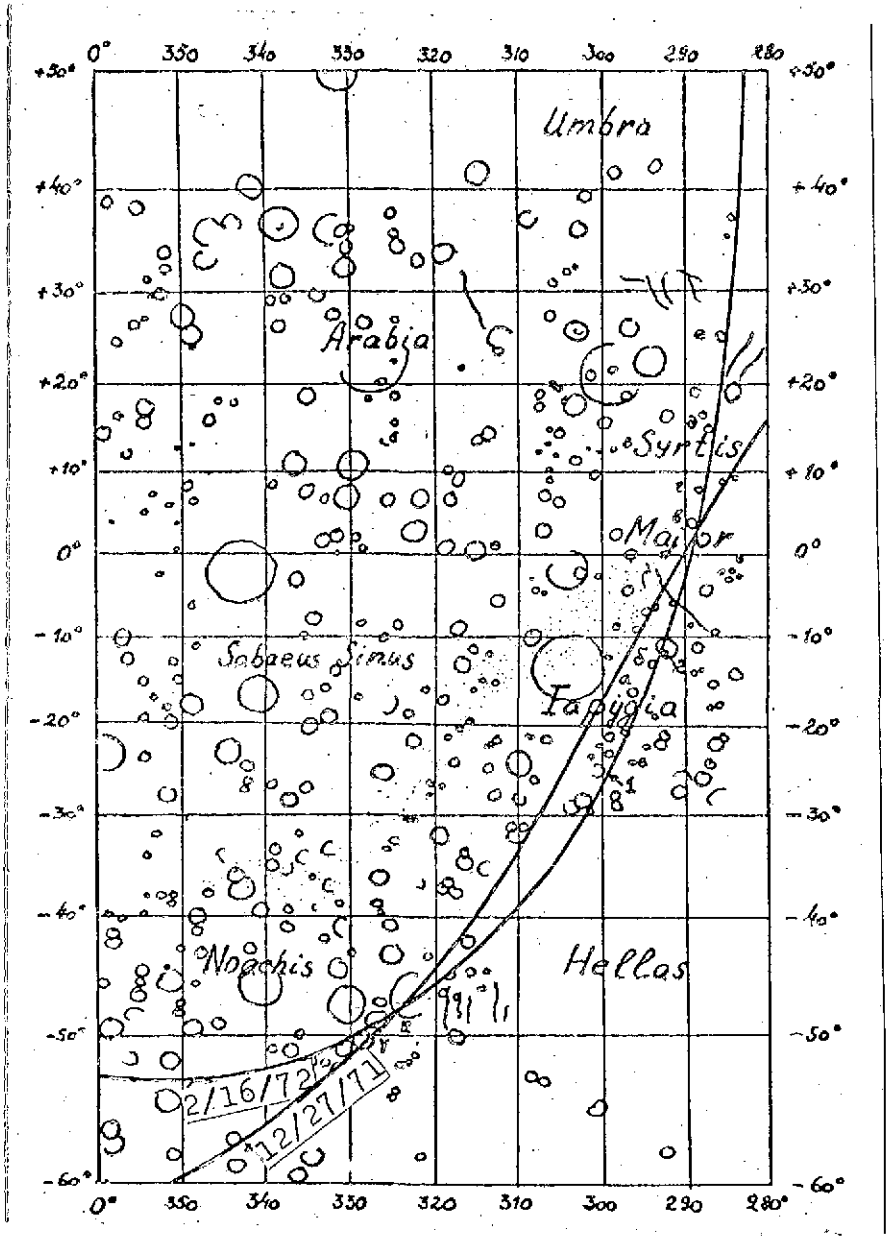

Figure 3. Same as Figure 2, for the scans of December 27 and February 16

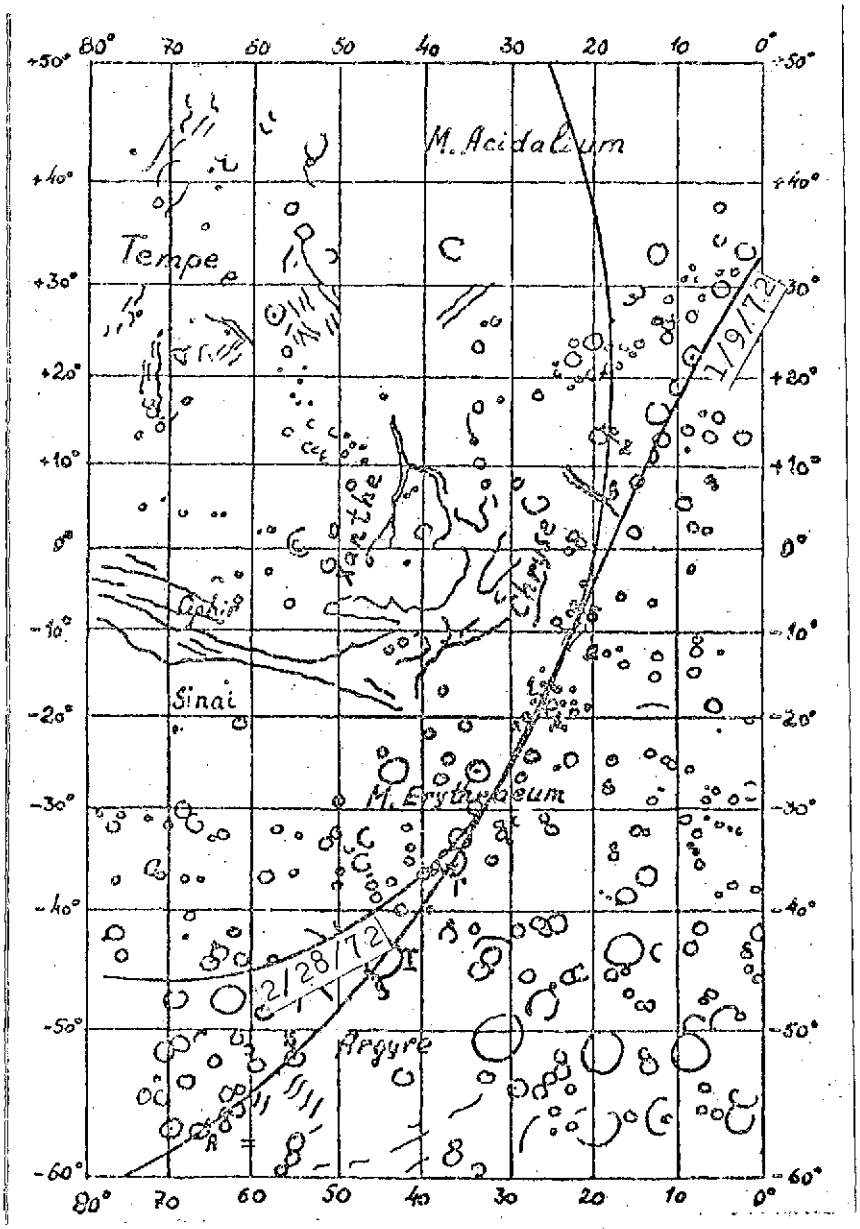

Figure 4. Same as Figure 2, for the scans of January 9 and February 28

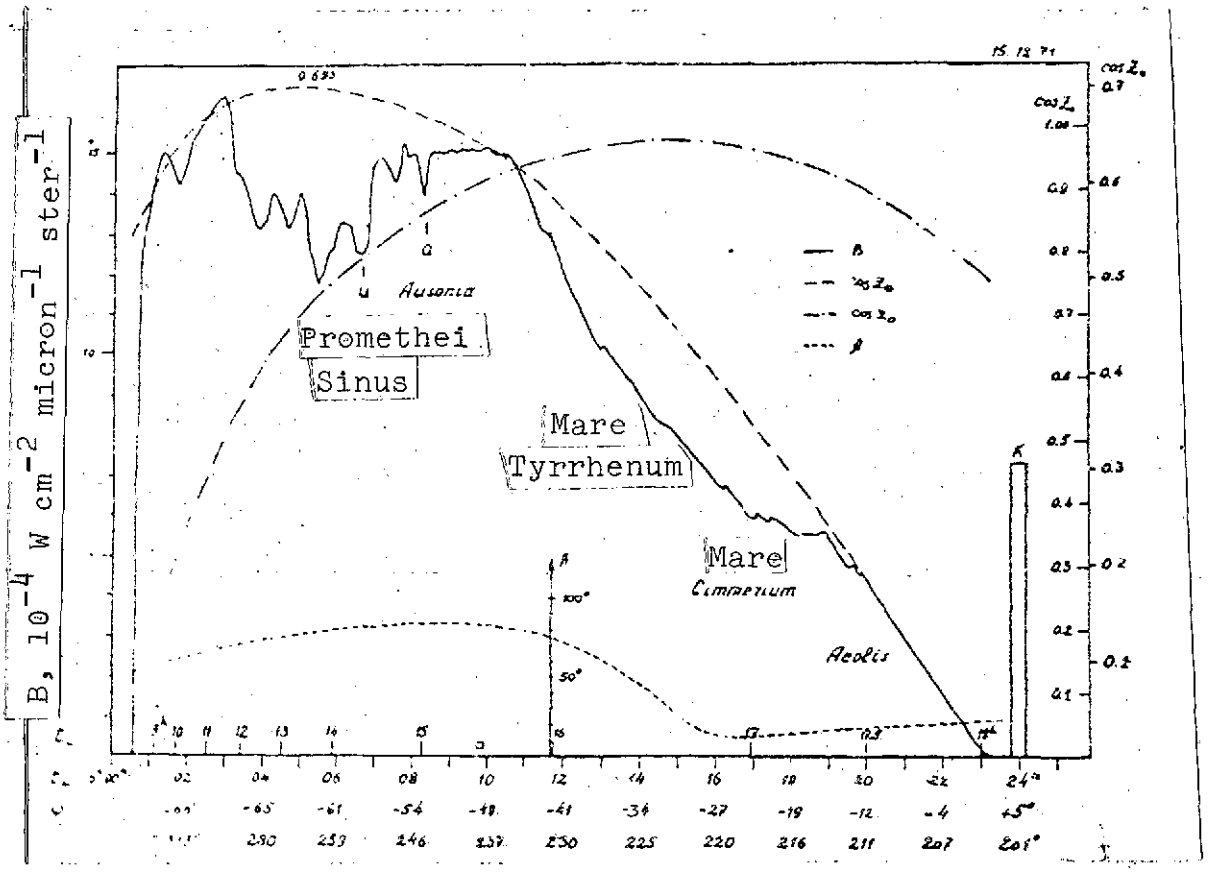

Figure 5. Photometric profile at wavelength of 1.38 microns for the scan of December 15. Cosines of angles of incidence (μ_1) and reflection (μ_2) are given here, plus the azimuthal angle between the planes of incidence and reflection. At the beginning or end of the profile is a calibration signal K. Along the abscissa axis the Moscow time t_M, the local solar time on Mars t_i, the latitude φ, and longitude λ are indicated. The unit along the ordinate axis is the absolute surface brightness

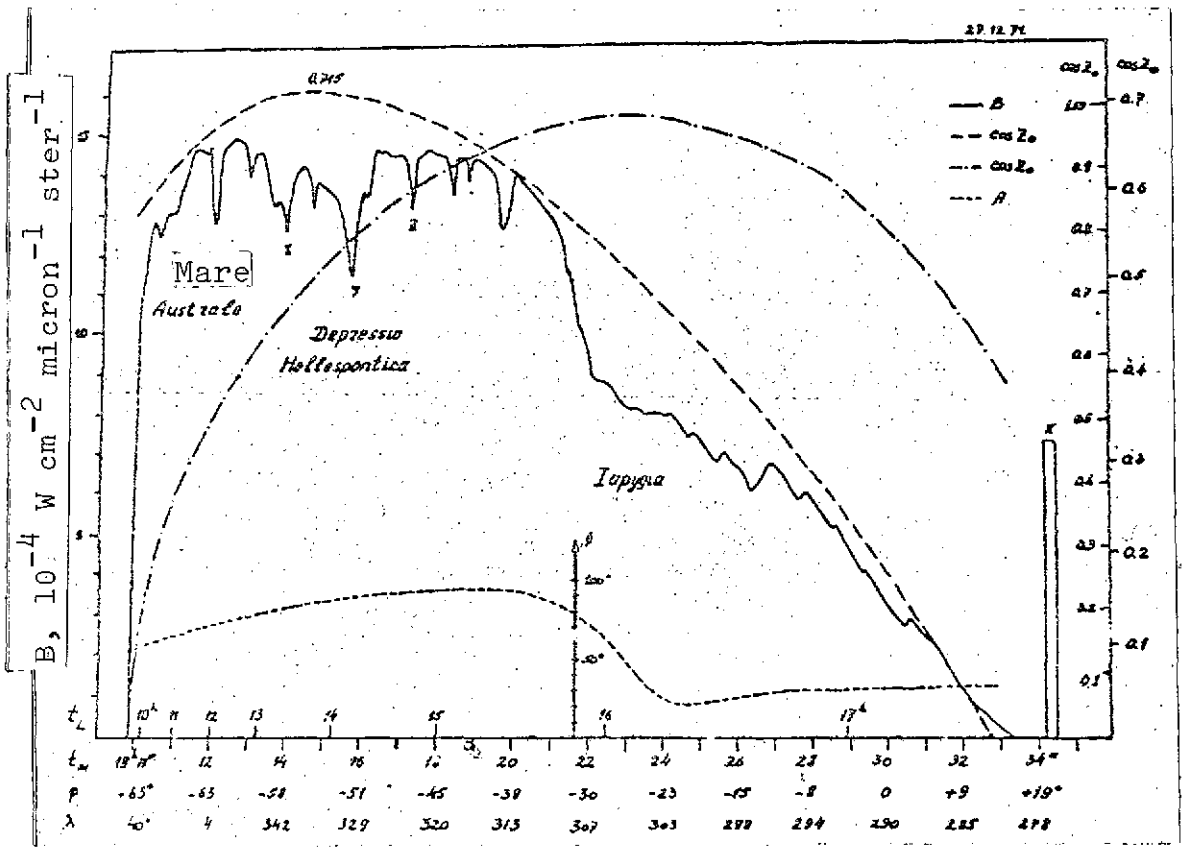

Figure 6. Same as Figure 5, for the scan of December 27

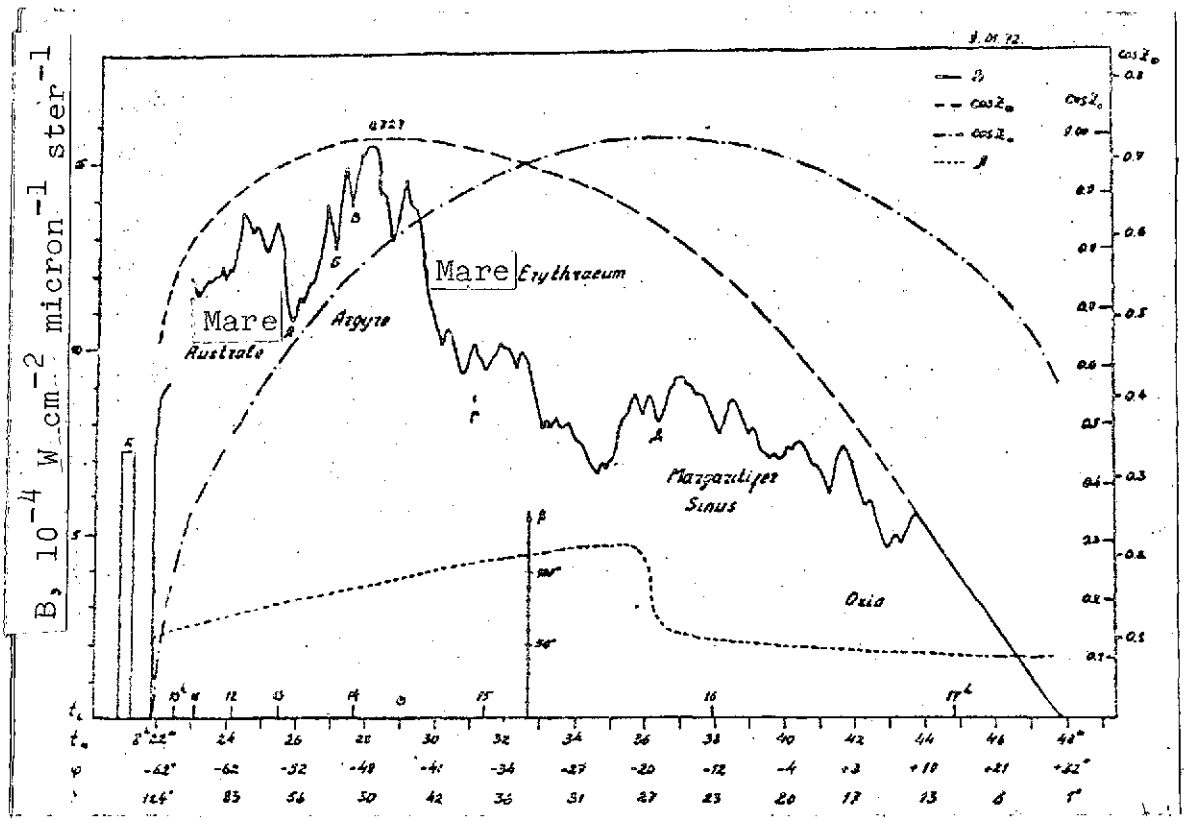

Figure 7. Same as Figure 5, for the scan of January 9

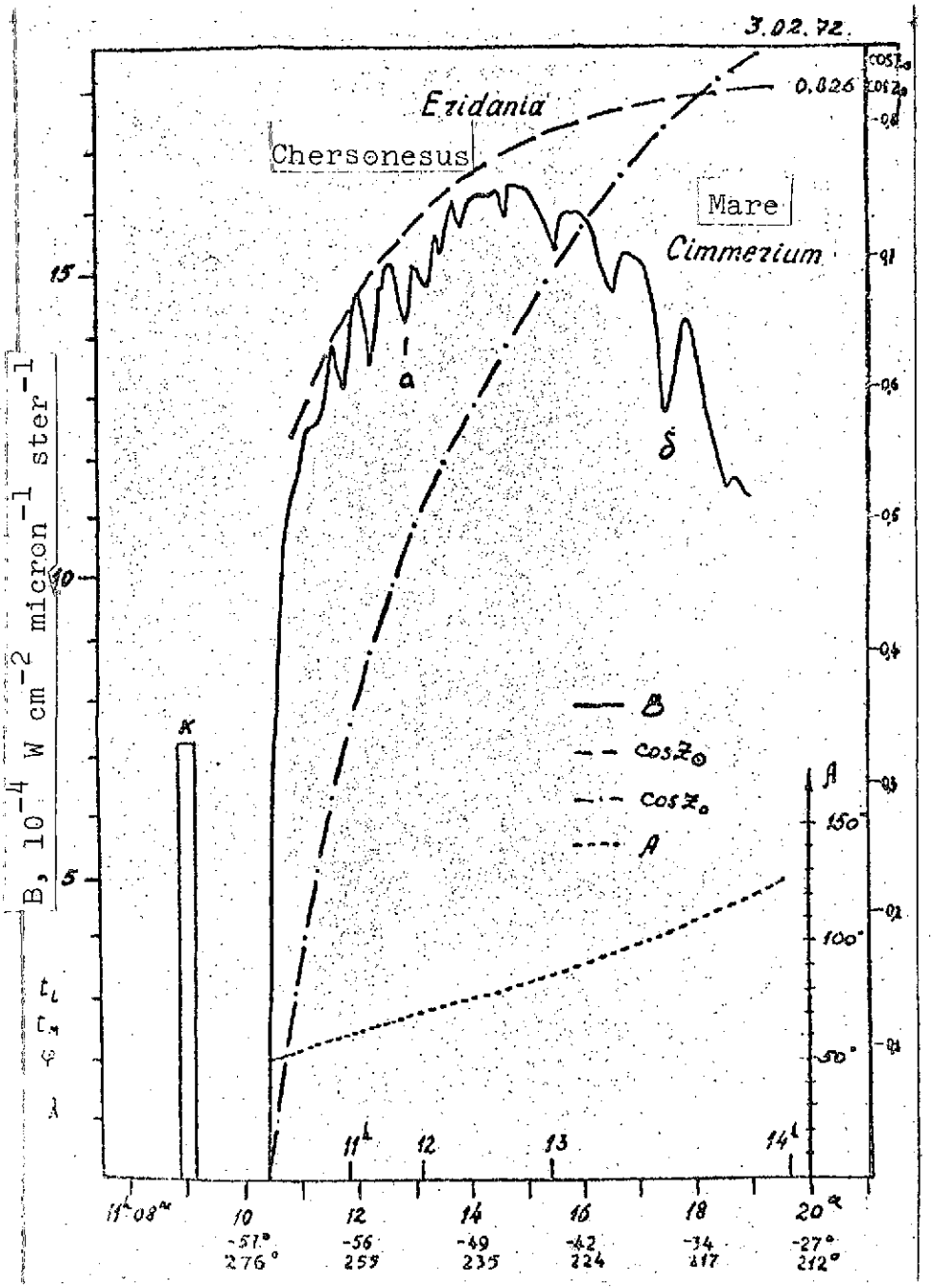

Figure 8. Same as Figure 5, for the scan of February 28

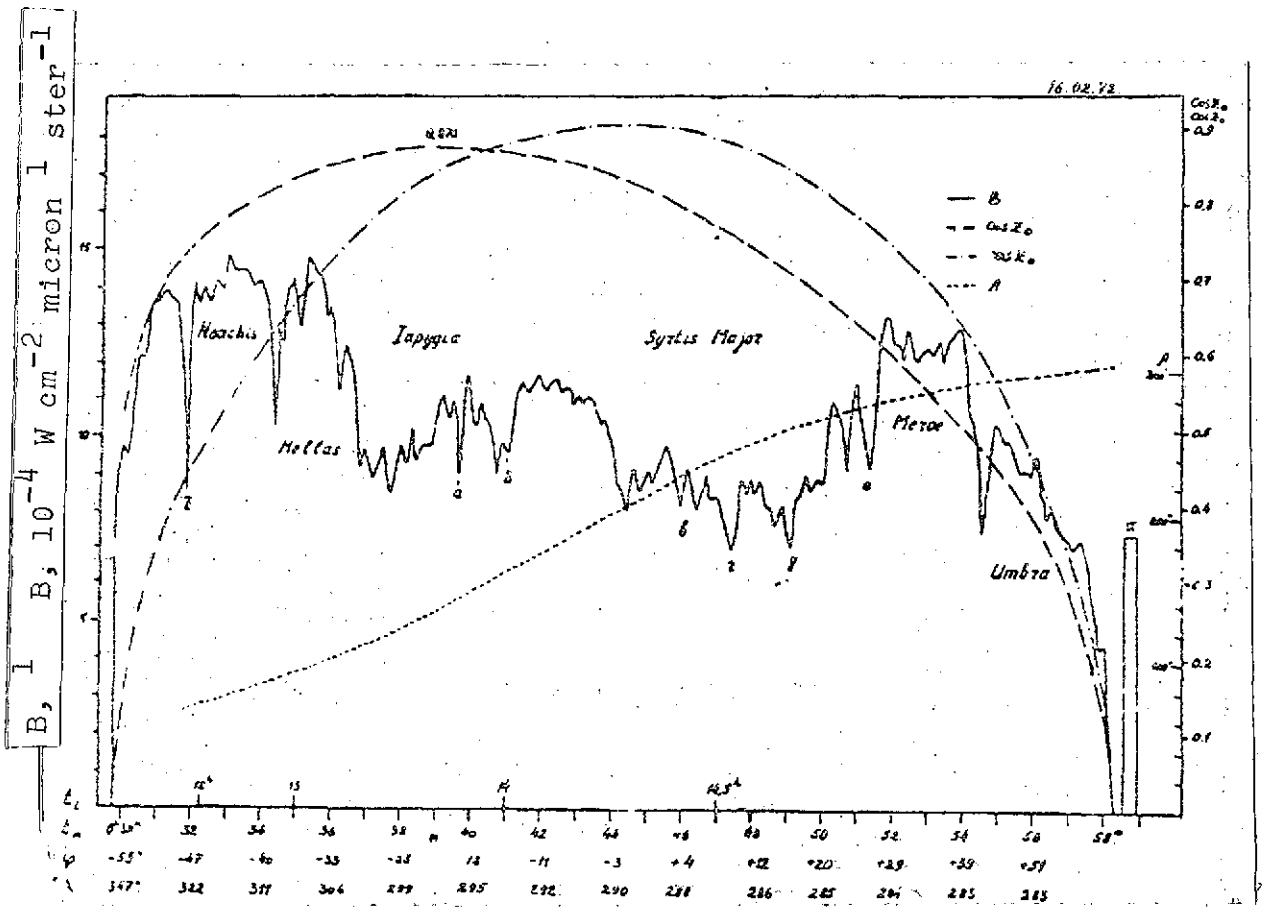

Figure 9. Same as Figure 5, for the scan of February 16

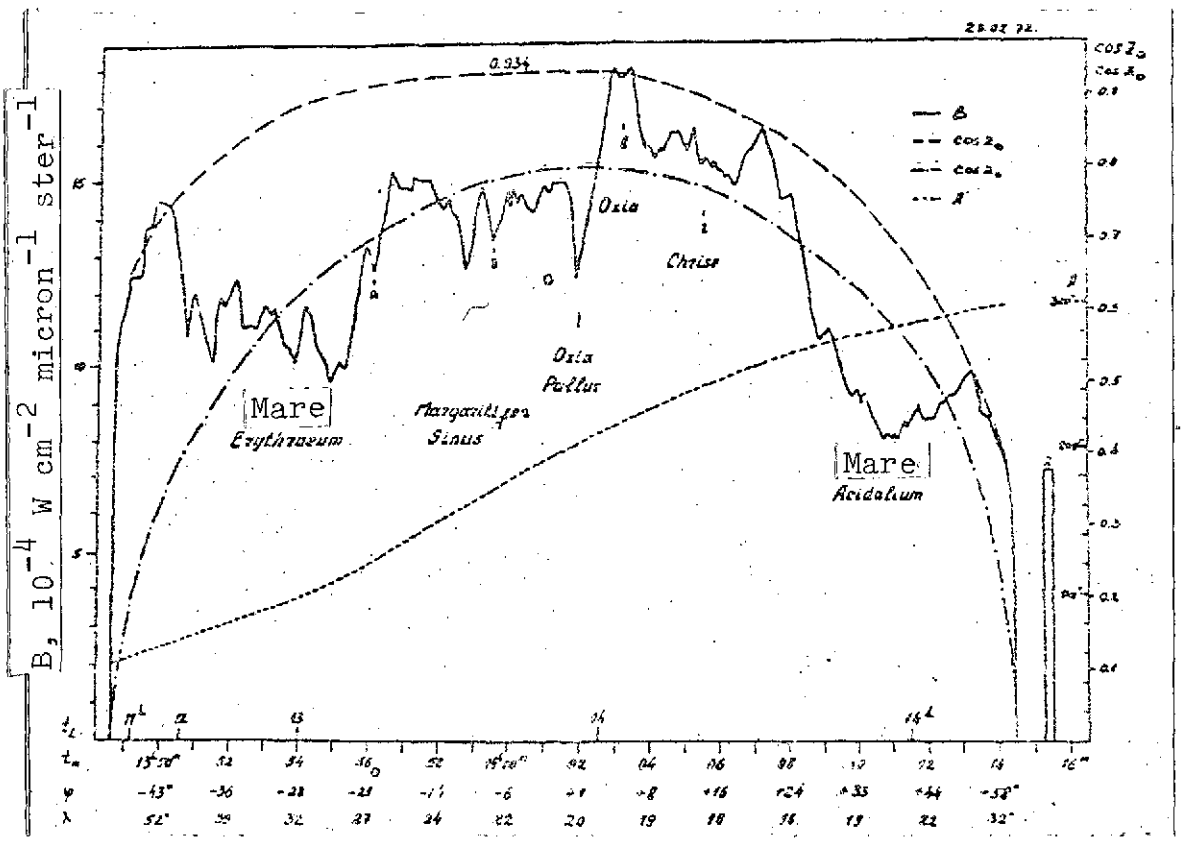

Figure 10. Same as Figure 5, for the scan of February 28

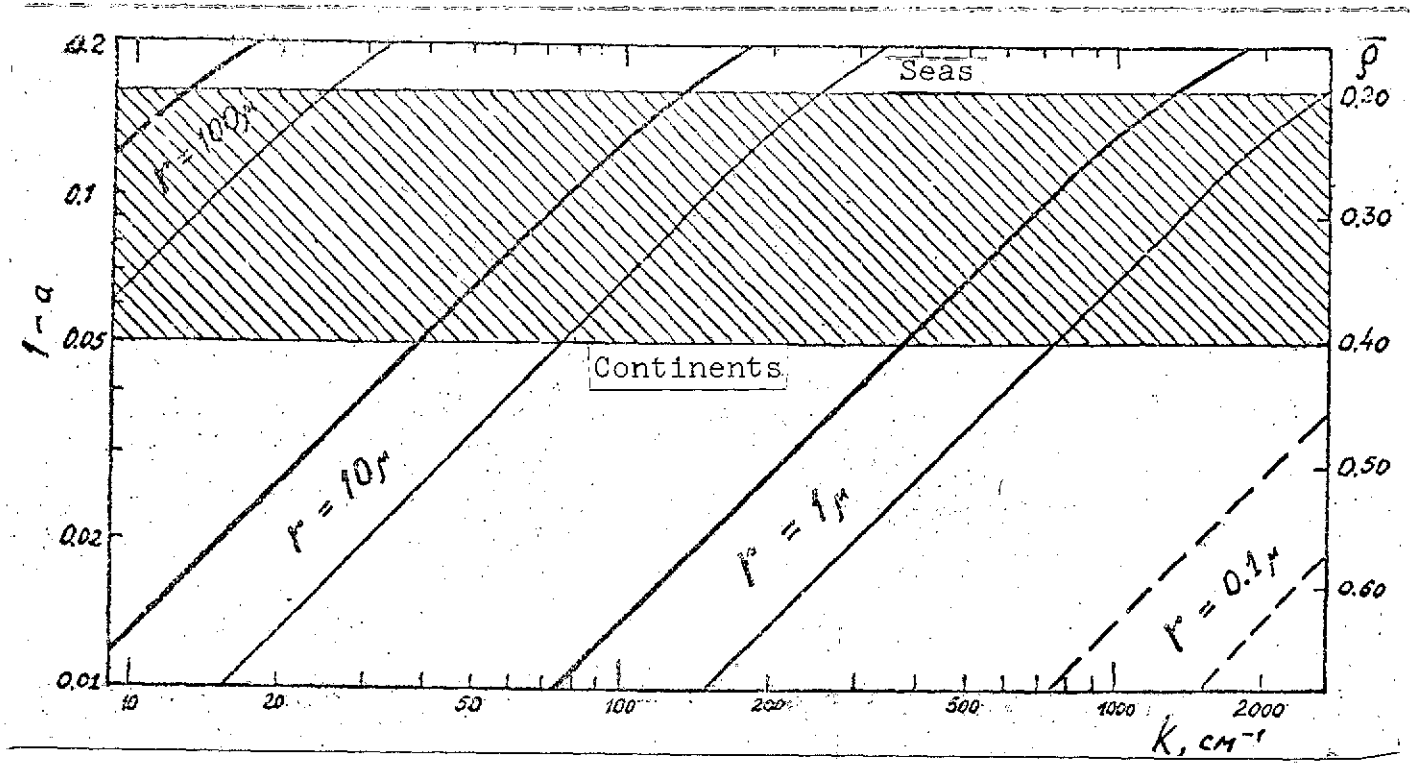

Figure 11. Dependence of the single-scattering albedo parameter (a) and normal albedo (ρ_0) of a semi-infinite layer on the volume absorption coefficient (k) and particle radius (r). For each radius case, the thicker curve refers to lightly packed granules [Equation (8)], and the thinner curve to dense packing [diffraction neglected, i.e., Equation (9) with R = 0]

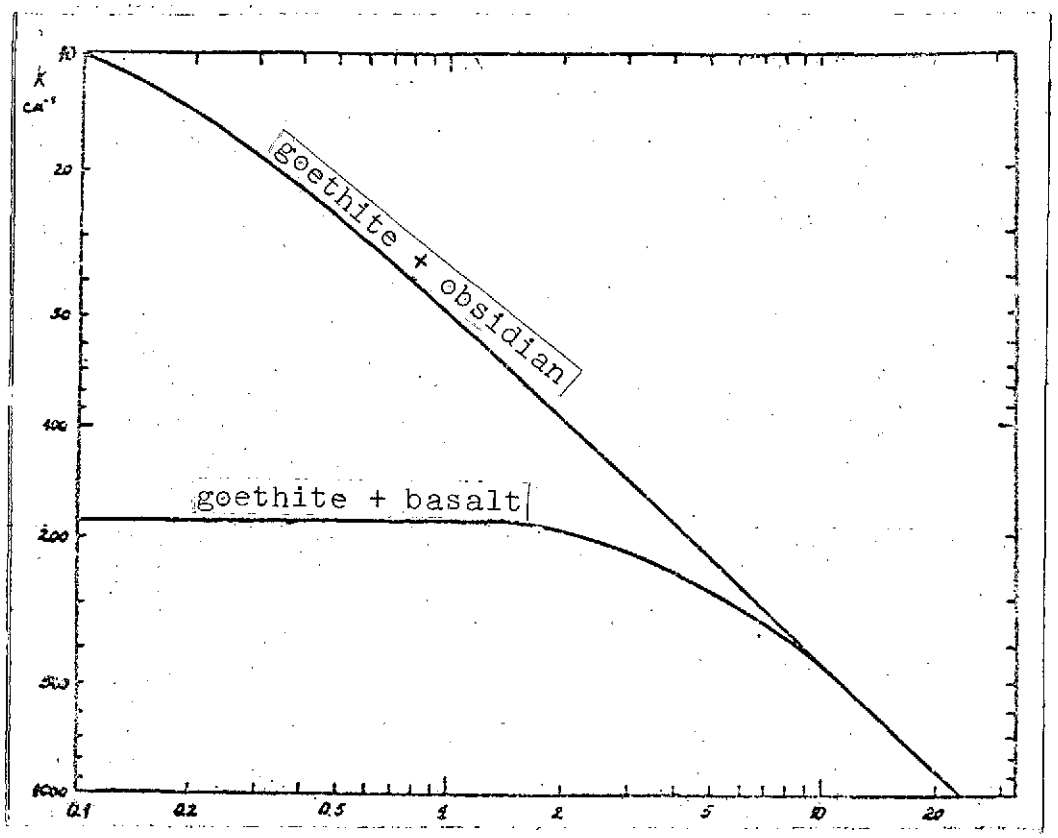

Figure 12. Dependence of the volume absorption coefficient (k) on goethite content for mixtures of goethite plus basalt and goethite plus obsidian

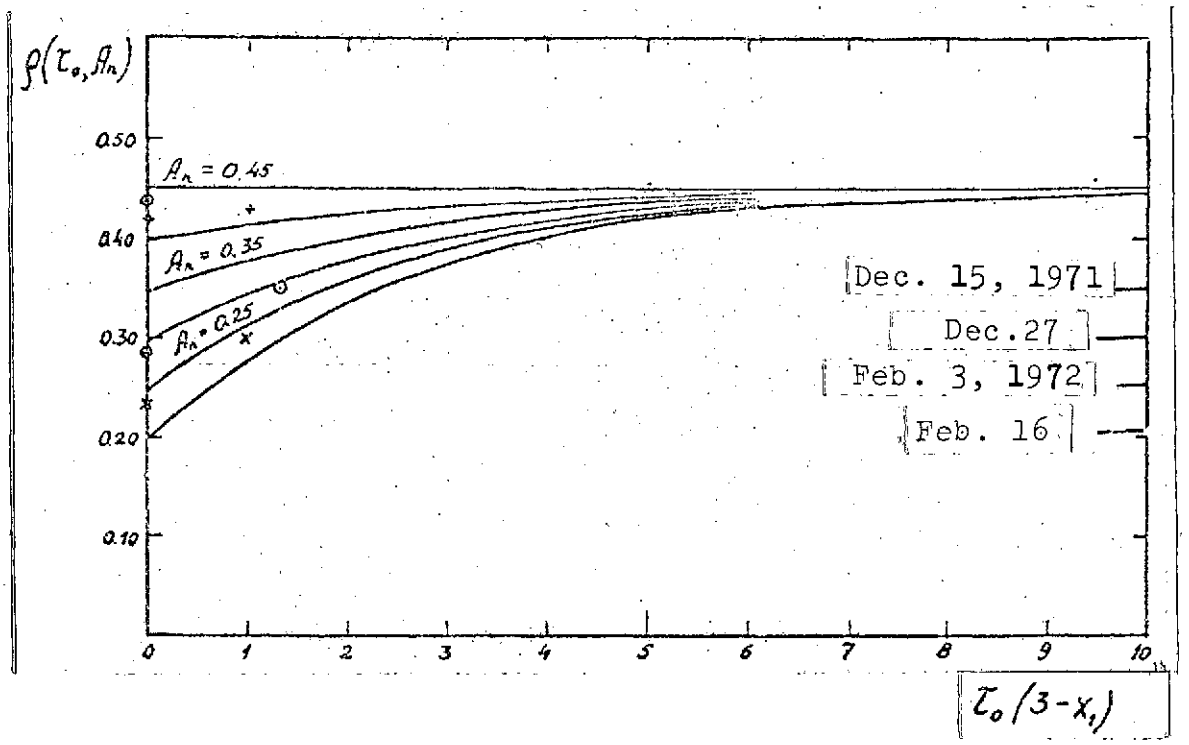

Figure 13. Reflectivity coefficient of the planet averaged over azimuth ($\rho(\tau_0, A_n)$) for regions covered by clouds with moderate optical depth A_n; (τ_0) is the surface albedo.

Circled points and crosses give values of ρ and $\tau_0(3-\varkappa_1)$ corresponding to the observations. The theoretical curves correspond to the case $\rho(\infty, A_n) = 0.45$

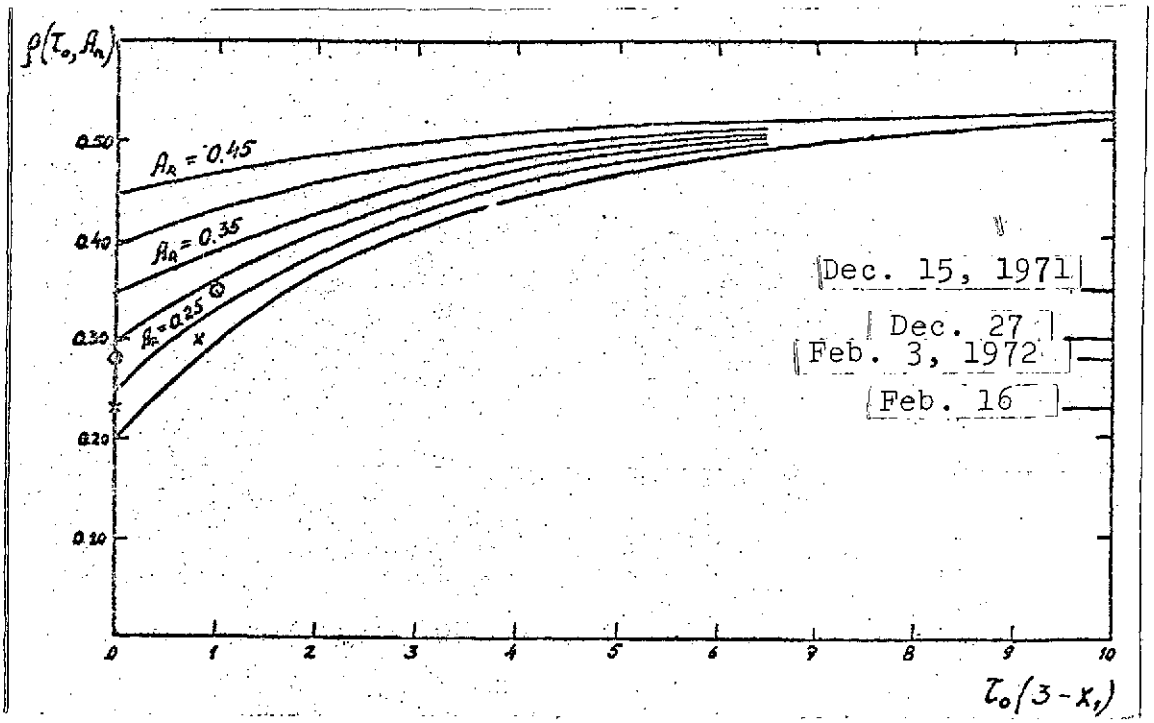

Figure 14. Same as Figure 13, but with theoretical curves for the case $\rho(\infty, A_n) = 0.53$

REFERENCES

1. Minnaert, M. Astroph. J., Vol. 93, 1941, p. 403. /20

2. Sytinskaya, N. N. Uch. Zapiski L.G.U., No. 116, 1949, p. 123.

3. Sytinskaya, N. N. Doklady akademiya nauk SSSR, Vol. 43, 1944, p. 151.

4. Fesenkov, V. G. Astronomicheskiy Zhurnal, Vol. 21, 1944, p. 257.

5. Barabashev, N. P. and I. K. Koval'. Fotograficheskaya fotometriya Marsa so svetofil'trami v 1956 (Photographic Photometry of Mars with Color Filters in 1956). Izdaniya KhGU, 1959.

6. Barabashev, N. P. and I. K. Koval'. Rezul'taty nablyudeniy Marsa vo vremya velikogo protivostroyaniya 1956 (Observational Results for Mars During the Close Opposition of 1956). Izdaniya AN SSSR, Vol. 10, 1959.

7. Bugayenko, L. A., O. I. Bugayenko, I. K. Koval' and A. V. Morozhenko. Fizika planet i luny (Physics of the Planets and the Moon). Naukova Dumka, Kiev, 1964.

8. Moroz, V. I., A. E. Nadzhip, A. B. Gil'varg, V. A. Korolev and V. C. Zhegulev. Doklady akademiya nauk SSSR, No. 208, 1973, p. 797.

9. Dollfus, A. and J. Focas. C. R. Acad. Sci., Paris, No. 262, 1967, p. 1024.

10. Mariner-9 Television Experiment Team. Sky and Tel., Vol. 44, 1972, p. 77.

11. Moroz, V. I. and L. V. Ksanfomality. Icarus, Vol. 17, 1972, p. 408.

12. Moroz, V. I., L. V. Ksanfomality, A. M. Kasatkin and A. E. Nadzhip. Kosmicheskiye issledovaniya, Vol. 10, 1972, p. 925.

13. McCord, T. B. and J. A. Westphal. Astrophys. J., Vol. 168, 1971, p. 141.

14. Ksanfomality, L. V., V. I. Moroz, B. C. Kunashiv and V. C. Zhegulev. Mars-3: davleniya i vysoty po rezul'tatam CO_2-al'timetrii (Mars-3: Pressure Versus Altitude from the Results of CO_2-Altimitry). (Preprint). IKI (Institut kosmicheskikh issledovanii) akademiya nauk SSSR, 1974.

15. Sagen, C., J. Veverka, P. Fox et al. Icarus, Vol. 17, 1972, p. 346.

16. Kieffer, H. H., S. C. Shase, Jr., E. Miner, G. Muench and G. Neugebauer. J.G.R., Vol. 78, 1973, p. 4251.

17. Moroz, V. I., L. V. Ksanfomality, G. I. Krasovskiy, et al. /21
Mars-3: infrakrasnyye temperatury i teplovyye svoystva poverkhnosti planety (Mars-3: Infrared Temperatures and Specific Heat of the Martian Surface). (Preprint). IKI akademiya nauk SSSR, 1974.

18. Irwine, W. M. J.G.R., Vol. 71, 1966, p. 2931.

19. Rosenberg, G. V. Doklady akademiya nauk SSSR, Vol. 145, 1962, p. 775; Collection: "spektroskopiya rasseivayushchikh sred" (Spectroscopy of scattering media), Minsk, 1963.

20. Sobolev, V. V. Rasseyaniye sveta v atmosferakh planet (Scattering of Light in Planetary Atmospheres). Nauka Press, Moscow, 1972.

21. Moroz, V. I. Fizika planet (Physics of the Planets). Nauka Press, Moscow, 1967.

22. Pollack, J. B. and C. Sagan. Sp. Sci. Rev., Vol. 9, 1969, p. 243.

23. Dollfus, A. Planets and Satellites, ed. G. P. Kuiper and B. M. Middlehurst. Chicago: University of Chicago Press, 1961, Chapters 9 and 15.

24. Hanel, R. A., R. J. Conrath, W. A. Hovis et al. Icarus, Vol. 17, 1972, p. 423.

25. Egan, W. and J. Becker. Appl. Opt., Vol. 8, 1969, p. 720.

26. Pollack, J. B., O. B. Toon and B. N. Khare. Icarus, Vol. 19, 1973, p. 372.

27. Moroz, V. I. Oblaka na Marse: nekotoryye vyvody iz nablyudeniy na Marse-3 (Some Conclusions from Mars-3). (Preprint). IKI akademiya nauk SSSR, 1974.

28. Moroz, V. I. O strukture marsianskogo grunta po opticheskim i infrakrasnym nablyudeniyam (On the Structure of the Martian Soil from Optical and Infrared Observations). (Preprint). IKI akademiya nauk SSSR, 1974.

Translated for National Aeronautics and Space Administration under contract No. NASw 2483, by SCITRAN, P. O. Box 5456, Santa Barbara, California, 93108